Original Article | Open Access

Microbiome Research Reports

Pei *et al. Microbiome Res Rep.* 2026;5:31 **DOI:**10.20517/mrr.2026.47

Prolonged supplementation with *Lactiplantibacillus plantarum* alleviates age-associated phenotypes in mice

Yang Pei[1], Shaoyang Ni[2], Jin Yang[2], Rui Chen[2], Jingjing Wang[3], Yang Liu[2], Xiaoting Luan[2], Wenye Huang[2], Xuetong Shen[4], Xingyin Liu[1,2]

Keywords:
Lactiplantibacillus plantarum L168, aging, probiotics, gut-brain axis, intestinal barrier, immunosenescence, neuroplasticity

Citation: Pei Y, Ni S, Yang J, Chen R, Wang J, Liu Y, Luan X, Huang W, Shen X, Liu X. Prolonged supplementation with *Lactiplantibacillus plantarum* alleviates age-associated phenotypes in mice. *Microbiome Res Rep.* 2026;5:31. https://dx.doi.org/10.20517/mrr.2026.47

Received: 9 Jul 2026 **First Decision:** 5 Aug 2026 **Revised:** 4 Nov 2026 **Accepted:** 6 Nov 2026 **Published:** 23 Nov 2026

Academic Editor: Clara G. de los Reyes-Gavilán
Copy Editor: Shu-Yuan Duan
Production Editor: Shu-Yuan Duan

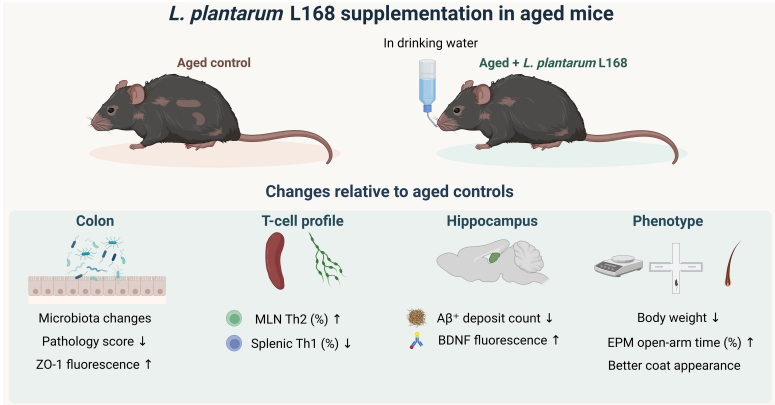

Abstract

Background: Intestinal barrier impairment, persistent inflammation and neurobehavioral decline accompany aging. Whether prolonged supplementation with a specific probiotic strain modifies these phenotypes remains unclear. We examined long-term *Lactiplantibacillus plantarum* L168 supplementation in naturally aged female mice, assessing behavior, intestinal histology, tissue-associated microbiota, cytokine-positive Cluster of differentiation 4-positive ($CD4^+$) T-cell frequencies and hippocampal molecular features.

Methods: Twelve-month-old female C57BL/6 mice received drinking water supplemented with *L. plantarum* L168 for 12 months. Behavioral testing, colonic histology, flow cytometry, hippocampal RNA sequencing and immunofluorescence were used to assess physiological, immune and neurological outcomes. Tissue-associated microbiota were profiled by five-region 16S rRNA gene sequencing of formalin-fixed, paraffin-embedded colon tissue.

[1]Department of Biochemistry, SUSTech Homeostatic Medicine Institute, School of Medicine, Department of Pediatrics, Foshan Hospital Affiliated to Southern University of Science and Technology, Southern University of Science and Technology, Shenzhen 518055, Guangdong, China.
[2]State Key Laboratory of Reproductive Medicine and Offspring Health, Jiangsu Province Center of Global Health, Nanjing Medical University, Nanjing 211166, Jiangsu, China.
[3]Department of Gastroenterology, Nantong Third People's Hospital, Nantong 226000, Jiangsu, China.
[4]Institute of Cancer Research, Shenzhen Bay Laboratory, Shenzhen 518055, Guangdong, China.

Correspondence to: Prof. Xingyin Liu, Department of Biochemistry, SUSTech Homeostatic Medicine Institute, School of Medicine, Department of Pediatrics, Foshan Hospital Affiliated to Southern University of Science and Technology, Southern University of Science and Technology, Shenzhen 518055, Guangdong, China; State Key Laboratory of Reproductive Medicine and Offspring Health, Jiangsu Province

Center of Global Health, Nanjing Medical University, Nanjing 211166, Jiangsu, China. E-mail: liuxingyin@sustech.edu.cn

Results: Long-term *L. plantarum* L168 supp lementation was associated with lower endpoint body weight, altered colonic histology and zonula occludens-1 (ZO-1) staining, and tissue-specific differences in cytokine-positive $CD4^+$ T-cell frequencies. Supplemented mice spent a higher proportion of time in the open arms of the elevated plus maze and showed lower hippocampal amyloid-β immunoreactivity. Morris water maze outcomes did not differ significantly between groups. Hippocampal transcriptomics yielded exploratory signals related to neural and immune processes. Microbial diversity and overall community structure did not differ significantly, although nine genera showed nominal differences; no predicted functional pathway remained significant after false discovery rate (FDR) correction.

Conclusion: Long-term supplementation with *L. plantarum* L168 was associated with favorable intestinal, microbial, immune, behavioral, and hippocampal changes in naturally aged female mice. These findings suggest that *L. plantarum* L168 may support health in later life, although studies incorporating young reference animals and longitudinal assessments are needed to determine whether it modifies age-related trajectories.

INTRODUCTION

Aging is a complex biological process characterized by a progressive decline in physiological functions, including metabolic regulation, immune responses, and behavioral performance[1-3]. These changes not only compromise overall health but also increase the risk of age-related diseases[4,5]. In recent years, the gut microbiota has emerged as a potential contributor to age-related physiology because of its influence on host physiological functions[6,7]. The gut microbiota has been implicated in age-related physiological changes through its roles in immune modulation and maintenance of intestinal homeostasis[6,8,9]. Aging has been associated with alterations in microbial diversity and community composition, which have been closely linked to impaired gut barrier function, systemic inflammation, and altered innate immune function[10].

Probiotic supplementation has been investigated as a strategy to modify age-related host physiology through effects on the gut microbiota[11]. In cyclophosphamide-treated mice, *Lactiplantibacillus plantarum* supplementation has been reported to alter gut microbial composition and intestinal immune markers[12]. *L. plantarum* L168 and its metabolite indole-3-lactic acid have been investigated in mouse models of colorectal tumorigenesis[13]. *L. plantarum* L168 has also been studied in hyperoxia-induced pulmonary inflammation and hypoalveolarization in neonatal rats[14]. Separately, *L. plantarum* L168 and its derived sodium benzoate have been investigated in offspring of mice exposed to maternal immune activation, with reported effects on social behavior and astrocyte-associated molecular processes[15].

However, the long-term, strain-specific effects of *L. plantarum* L168 in natural aging remain insufficiently characterized. To address this gap, we conducted a 12-month intervention in 12-month-old female mice. We integrated endpoint measurements of body weight and gross appearance with behavioral, intestinal, immunological, microbiome, and hippocampal analyses to characterize treatment-associated differences.

MATERIALS AND METHODS

Mice

Nanjing Medical University supplied the female C57BL/6 mice, which were twelve months old at enrollment. Females were selected to reduce aggression-related injury and attrition during 12 months of group housing. The specific pathogen-free housing facility maintained a temperature of 22 ± 1 °C, humidity of 50%-60% and

a 12-h light/dark cycle. Water and a specific pathogen-free (SPF)-grade laboratory animal compound diet formulated for Nanjing Medical University were freely available. Forty mice were individually randomized by drawing lots to aged control or *L. plantarum* L168 supplementation (20 per group), then housed five per cage without additional enrichment. No a priori power calculation was performed. Outcome acquisition, assessment and data analysis were blinded to group assignment where applicable. Mortality reduced the cohort to 12 mice per group. One additional *L. plantarum* L168-supplemented mouse died before Morris water maze (MWM) and terminal body-weight assessments, leaving 12 control and 11 supplemented mice for these endpoints. For assays requiring fewer mice, animals were randomly selected from the surviving cohort. Final sample sizes (control/*L. plantarum* L168) were elevated plus maze (EPM), 12/12; open field, 12/12; MWM, 12/11; body weight, 12/11; colorectal length, 5/5; histopathology, 10/8; zonula occludens-1 (ZO-1) immunofluorescence, 7/7; hippocampal amyloid-β (Aβ)/ brain-derived neurotrophic factor (BDNF) immunofluorescence, 5/5; flow cytometry, 6/6; 16S rRNA sequencing, 11/11; and RNA-seq, 5/5. All collected samples were analyzed without technical exclusions. Prespecified humane endpoints were severe wasting, inability to eat or drink, persistent weakness and impaired mobility. No mouse reached these endpoints or was euthanized on these grounds; individual causes of death were not determined. The Nanjing Medical University Institutional Animal Care and Use Committee approved the animal procedures (IACUC-2006031).

Bacterial preparation and administration

L. plantarum L168 was isolated from the intestinal tract of *Drosophila melanogaster* and deposited at the China General Microbiological Culture Collection Center (CGMCC No. 13660; 13 February 2017). Its identity was characterized by colony morphology, Gram staining, biochemical profiling, 16S rRNA gene sequencing, multilocus sequence typing and whole-genome sequencing[16]. To maintain purity, the preserved culture was streaked weekly on MRS agar, and an isolated colony was reactivated. Anaerobic culture in de Man, Rogosa and Sharpe (MRS) broth proceeded at 37 °C until optical density at 600 nm (OD_{600}) reached 0.8-1.0. After centrifugation, the cells underwent two washes in sterile phosphate-buffered saline (PBS) before resuspension at an OD_{600}-based estimate of 1×10^9 colony-forming units (CFU)/mL. Mice received 1 mL of this suspension in 100 mL of sterile drinking water ad libitum, giving a nominal initial concentration of 1×10^7 CFU/mL. Fresh supplemented water was supplied every 48 h for 12 months. Controls received 1 mL of sterile PBS per 100 mL of drinking water. Water consumption was not recorded at either cage or individual level, and bacterial viability was not measured over the 48-h interval. Actual daily viable intake per mouse was therefore unknown.

Morris water maze

The MWM followed published protocols for spatial learning and memory assessment[17,18]. A circular pool measuring 120 cm in diameter and 50 cm in height held opaque water. The 9-cm-diameter escape platform lay 1 cm beneath the surface. An automated system from Shanghai XR Information Technology Co., Ltd. (China) tracked the mice. Controls (n = 12) and *L. plantarum* L168-treated mice (n = 11) underwent four trials daily on days 1-3. Starting quadrants were assigned pseudo-randomly, and each mouse initially faced the pool wall. Each trial measured escape latency with a 60-s cutoff. Mice that did not locate the platform were guided there and remained on it for 10 s. The day-4 probe trial lasted 60 s without the platform. Release from the opposite quadrant allowed measurement of target-quadrant time and crossings of the former platform location.

Elevated plus maze

Published elevated plus maze protocols were used to evaluate anxiety-like behavior[19,20]. The apparatus stood 50 cm above the floor, with open arms measuring 30 cm × 5 cm and enclosed arms measuring 30 cm × 5 cm × 15 cm, two of each. Each mouse began at the central intersection, oriented toward an open arm, and

explored the apparatus for 5 min. Automated tracking (Shanghai XR Information Technology) measured the percentages of time and distance in open arms and counted entries into both arm types. Between animals, the apparatus was cleaned using 70% ethanol.

Open field test

Open-field behavior was assessed using published procedures[21,22], with the arena layout and representative tracks shown in Supplementary Figure 1A. Mice explored an opaque-walled arena (50 cm × 50 cm × 40 cm) for 5 min under uniform illumination, starting from the center. Automated tracking recorded distance, time and entries in the peripheral and center zones, each expressed as a proportion of its corresponding total. These measures were examined for potential locomotor confounding of MWM and EPM outcomes. The arena was cleaned with 70% ethanol between mice.

Colon length, histology, and immunofluorescence

After euthanasia, colorectal length was measured from cecum to rectum without tension. Following fixation in 4% paraformaldehyde and paraffin embedding, 5-μm sections were prepared for hematoxylin and eosin (H&E) staining. A NanoZoomer® S360 scanner (Hamamatsu Photonics), equipped with a 20× objective, captured the stained sections. One blinded observer scored one section and one panoramic field per mouse. The composite score (0-16) comprised inflammation (0-4), tissue-structure damage (0-4), submucosal changes (0-3), glandular destruction (0-3) and other special pathological changes (0-2). Higher scores indicated more severe lesions. The ZO-1 protocol began with antigen retrieval in citrate buffer (pH 6.0) and blocking in 5% bovine serum albumin (BSA). Anti-ZO-1 (Proteintech, 1:200) was incubated overnight at 4 °C. Subsequent steps comprised a 1-h incubation at room temperature with Alexa Fluor-conjugated secondary antibodies (1:500) and 4′,6-diamidino-2-phenylindole (DAPI) counterstaining. One section per mouse from seven mice per group was imaged with a 40× objective. Mean ZO-1 intensity was calculated from the complete Z-stack, yielding one value per mouse.

Hippocampal immunofluorescence. Deparaffinization involved heating the sections at 65 °C for 2-3 h, followed by xylene treatment (2 × 10 min). Rehydration proceeded through 100%, 95%, 70% and 50% ethanol, with 3 min at each concentration. For antigen retrieval, sections in 1× citrate buffer were microwaved for 10 min at high power and 15 min at medium power. After cooling for approximately 30 min, sections received three phosphate-buffered saline containing Tween 20 (PBST) washes (PBS, 0.1% Tween-20, 0.05% Triton X-100) and a 2-h block in 5% donkey serum. Separate sections received either anti-BDNF (Abcam, ab108319) or anti-β-Amyloid (1-42) (D9A3A; Cell Signaling Technology, 14974S) overnight at 4 °C. Both primary antibodies were diluted 1:500 in 3% BSA/PBS. Secondary labeling used both 488- and 647-conjugated antibodies at 1:500 for 2 h, protected from light at room temperature. Staining was evaluated in the 647 channel. DAPI-containing mounting medium was used, and the mounted sections were stored at -20 °C. One section per mouse was analyzed from five mice per group. Aβ-immunoreactive deposits were counted manually across the whole hippocampus using a 40× objective, yielding one count per mouse. BDNF was imaged with a 20× objective in one blindly selected field each from CA1, CA2-3 and DG. Mean intensity was calculated separately from each subregion's complete Z-stack. No-primary-antibody and isotype controls were not performed.

Images were acquired on a Zeiss LSM800 and analyzed in ZEISS Efficient Navigation(ZEN), with acquisition and quantification blinded to group assignment. Hippocampal acquisition settings were identical across groups. ZO-1 and BDNF Z-stacks covered the full visible tissue depth at 0.1-μm intervals. All immunofluorescence scale bars represent 20 μm.

Flow cytometry

Immediately after sacrifice, spleen and mesenteric lymph node (MLN) tissues were handled aseptically to prepare cell suspensions. Mechanical dissociation with a sterile syringe plunger preceded filtration through 70-μm strainers (BD Falcon). Cells were collected in chilled RPMI-1640 supplemented with 2% fetal bovine serum (FBS; Gibco). For splenic suspensions, ammonium-chloride-potassium (ACK) lysis buffer (Thermo Fisher Scientific) removed erythrocytes during a 3-min incubation at room temperature. Two washes in PBS with 2% FBS followed. All samples exceeded 90% viability by trypan blue exclusion, and the final concentration was 1×10^6 cells per 100 μL.

Cytokine assays began with a 5-h *ex vivo* stimulation of freshly isolated cells at 37 °C in 5% CO_2. The stimulation mixture contained PMA at 50 ng/mL, ionomycin at 500 ng/mL and brefeldin A at 5 μg/mL (Sigma). Washed cells received anti-CD16/32 (clone 93; BioLegend) for Fc-receptor blocking at 4 °C for 10 min. Zombie Aqua™ (BioLegend) was then used for viability staining as directed by the manufacturer. Surface labeling lasted 30 min, protected from light at 4 °C. The panel comprised PerCP-Cy5.5 anti-mouse CD45 (30-F11; BD Biosciences, 550994), fluorescein isothiocyanate (FITC) anti-mouse CD3ε (145-2C11; BD Biosciences, 553061) and phycoerythrin (PE)/Cyanine7 anti-mouse Cluster of differentiation 4 (CD4) (GK1.5; BioLegend, 100422). After washing, fixation and permeabilization were performed with the Foxp3/Transcription Factor Staining Buffer Set (Thermo Fisher Scientific, 00-5523-00). The intracellular panel comprised BV421 anti-mouse interferon-gamma (IFN-γ) (XMG1.2; BioLegend, 505829), PE anti-mouse interleukin-4 (IL-4) (11B11; Invitrogen, 12-7041-82) and allophycocyanin (APC) anti-mouse IL-17A (TC11-18H10.1; BioLegend, 506916). All three antibodies were combined in one tube for a 45-min incubation at 4 °C, protected from light. The Treg panel used unstimulated splenocytes labeled with APC anti-mouse CD25 (3C7; BioLegend, 101910) and PE anti-mouse Foxp3 (R16-715; BD Biosciences, 563101).

At least 50,000 total events per sample were acquired on a BD LSRFortessa™ using FACSDiva v8.0 and analyzed in FlowJo v10.8. Single-stained controls established compensation, fluorescence-minus-one (FMO) controls defined gates, and blank controls were included. Gating proceeded through lymphocytes (forward/side scatter), singlets, viable cells, $CD45^+$ cells and $CD3^+$ cells. Bivariate CD4/cytokine gates identified $CD4^+$IFN-γ^+, $CD4^+$IL-4^+ and $CD4^+$IL-$17A^+$ cells, each expressed as a percentage of viable $CD45^+CD3^+$ cells. Spleen and MLN samples from six mice per group were analyzed without exclusions.

DNA extraction and five-region 16S rRNA gene sequencing

Formalin-fixed, paraffin-embedded (FFPE) colon tissue served as the DNA source. Extraction followed the RC1102 high-sensitivity FFPE genomic DNA kit protocol (Kaishuo Biotechnology [Xiamen] Co., Ltd., Xiamen, China). Five sampling blanks, five DNA-extraction controls and five no-template PCR controls were included. Sequencing yields and quality-control metrics for all 15 controls are provided in Supplementary Table 1.

Multiplex PCR targeted five hypervariable regions within the bacterial 16S rRNA gene. The resulting amplicon libraries underwent sequencing on the Illumina NovaSeq 6000 platform.

Taxonomic profiling and bioinformatics

Reads were demultiplexed, quality-filtered and assigned to target regions by primer sequence. The Short Multiple Regions Framework (SMURF) algorithm[23] integrated the five regions using expectation-maximization to jointly estimate microbial community composition from reads spanning multiple 16S rRNA gene regions. Taxonomy and relative abundance were assigned using Greengenes2 (2024.09)[24]. Read counts were normalized per sample. Samples, including negative controls, with fewer than 1,000 reads and taxon observations with relative abundance below 10^{-4} were excluded. A TMB-based workflow (

https://github.com/ilivyatan/TMB) identified potential contaminants at a 30% prevalence threshold in negative controls. The experiment-associated and sampling-associated contaminant records are listed in Supplementary Table 2. Downstream analyses excluded these taxa and the control samples. Taxonomic profiles were aggregated at phylum and genus levels and converted to within-sample relative abundances. Phyla with mean abundance below 1% were grouped as 'Others'. The 10 genera with the highest mean abundance across all samples were retained; remaining genera were grouped as 'Others'. Composition plots show group means. Two-sided Wilcoxon rank-sum tests compared sample-level abundances of the top 10 genera and 'Others'. Genus-level Shannon indices were compared using a two-sided Welch's *t*-test. Genus-level Bray-Curtis dissimilarities and multivariate dispersion were assessed using permutational multivariate analysis of variance (PERMANOVA) and permutational analysis of multivariate dispersions (PERMDISP), respectively, each with 999 permutations. For genus-level differential abundance, two-sided Wilcoxon rank-sum tests identified taxa with $P < 0.05$ for the heatmap. These exploratory genus-level tests were not adjusted for multiple comparisons. Functional potential was inferred using Phylogenetic Investigation of Communities by Reconstruction of Unobserved States 2 (PICRUSt2; https://github.com/picrust/picrust2)[25]. Predicted MetaCyc pathway abundances were compared using two-sided Wilcoxon rank-sum tests with Benjamini-Hochberg false-discovery-rate correction. The five pathways with the smallest nominal *P* values were displayed in the heatmap.

Hippocampal RNA sequencing and bioinformatic analysis

Random selection from the surviving cohort yielded five mice per group for hippocampal RNA sequencing. For each mouse, the left and right hippocampi were combined immediately upon dissection and rapidly frozen in liquid nitrogen before storage at -80 °C. Libraries remained mouse-specific; tissue from different animals was never pooled. RNA isolation followed the supplier's protocol for TRNzol Universal Reagent (DP424; TIANGEN Biotech [Beijing] Co., Ltd., Beijing, China). An Agilent 2100 Bioanalyzer measured RNA integrity and quantity, and only RNA meeting RNA integrity number (RIN) ≥ 7.9 proceeded to library preparation. Oligo(dT) magnetic beads captured poly(A)+ mRNA, which was then fragmented. Random hexamers initiated first-strand cDNA synthesis before synthesis of the complementary strand. Library preparation continued with end repair and A-tailing, followed by adaptor ligation, fragment-size selection, amplification and purification. Novogene used the Illumina NovaSeq X Plus platform for paired-end sequencing, with a read length of 150 bp. The target yield per library was approximately 6 Gb of clean bases (20 million read pairs). Filtering with fastp[26] excluded adapter-containing, poly-N and low-quality reads; quality assessment included Q20, Q30 and guanine–cytosine (GC) content. HISAT2 v2.0.5[27] mapped reads to *Mus musculus* GRCm38/mm10, and featureCounts v1.5.0-p3[28] generated gene counts. DESeq2 v1.20.0[29] analyzed gene-level counts with treatment group as the sole model factor. Statistical significance was defined by $P < 0.05$. PCA used the FPKM matrix. All 10 libraries were prepared and sequenced in one batch and included in PCA and differential-expression analysis; no batch-correction term was used. Gene Ontology (GO) enrichment used clusterProfiler v3.8.1[30] with all detected genes as the background universe and unadjusted $P < 0.05$ as the threshold.

Quantification and statistical analysis

GraphPad Prism 10 and R v4.3.1 were used for the analyses. Values are summarized by the mean and its standard error (SEM). For two-group comparisons, the default tests were two-sided unpaired Student's *t*-tests, with Mann-Whitney *U* tests used for comparisons designated as nonparametric unless otherwise specified. The original records did not document a formal rule for choosing between these tests. For MWM acquisition, a two-way repeated-measures ANOVA included treatment group and training day as factors; repeated measurements belonged to individual mice. Normality, homogeneity of variance and sphericity were not formally tested; no sphericity correction was applied. PICRUSt2 pathway *P* values were Benjamini-Hochberg-adjusted; all other reported *P* values were unadjusted. The significance threshold was $P < 0.05$.

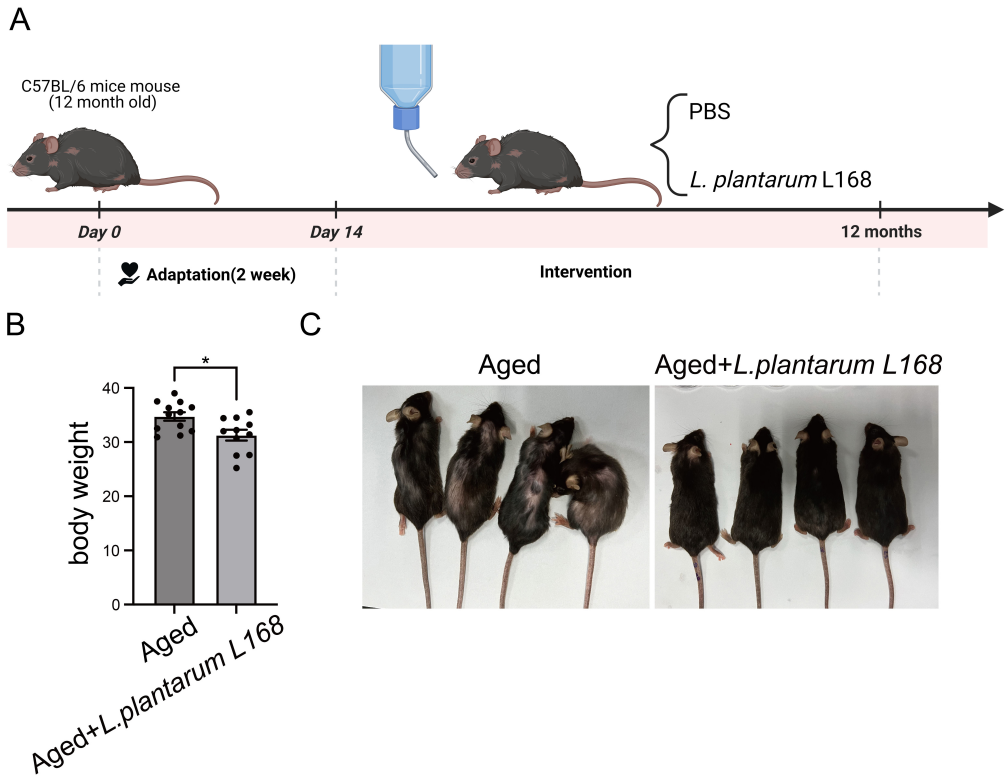

Figure 1. Experimental design and endpoint body-weight and gross-appearance comparisons. (A) Schematic representation of the experimental design. Twelve-month-old female C57BL/6 mice were allocated to an aged control group or an *L. plantarum* L168-supplemented group and received the assigned drinking water for 12 months. Created with BioRender; (B) Endpoint body weight (g) in aged control and *L. plantarum* L168-supplemented mice (control, $n = 12$; *L. plantarum* L168-supplemented, $n = 11$). Data are presented as mean ± SEM. Unpaired two-tailed Student's *t*-test, unadjusted $P = 0.0122$; $^*P < 0.05$; (C) Representative images of aged mice from each group showing differences in body size and hair quality. The images illustrate gross appearance at the endpoint; fur condition was not quantitatively scored. PBS: Phosphate-buffered saline; SEM: standard error of the mean.

Figure legends specify sample sizes and tests. The mouse was the independent biological unit for all analyses. Histology and fluorescence measurements yielded one value per mouse per endpoint or BDNF subregion; sections, imaging regions and Z-stack planes were within-mouse subsamples. Each RNA-seq library, tissue-specific flow-cytometry value and 16S rRNA sample represented one mouse.

RESULTS

L. plantarum L168 supplementation is associated with lower endpoint body weight and differences in gross appearance

We supplemented 12-month-old female C57BL/6 mice with *L. plantarum* L168 for 12 months and compared them with age-matched controls [Figure 1A]. At the endpoint, the *L. plantarum* L168-supplemented group had a lower mean body weight than the aged control group [Figure 1B]. However, without baseline or longitudinal body-weight data, the current comparison does not establish an effect on age-associated weight gain. We also examined gross appearance qualitatively. Representative images showed patchy hair loss in aged control mice and more extensive fur coverage in *L. plantarum* L168-supplemented mice [Figure 1C]. These observations were qualitative, as fur condition was not quantified. These endpoint observations describe treatment-associated differences in body weight and gross appearance.

Long-term *L. plantarum* L168 administration reduces anxiety-like behavior but does not improve spatial learning or memory in aged mice

Brain aging is associated with changes in cognitive function[31-33]. Studies of other *L. plantarum* strains with short-term supplementation have reported effects on cognition in animal models[34-36].

To further investigate the effects of long-term *L. plantarum* supplementation, we first assessed spatial learning and memory using the MWM as previously described [Figure 2A][17]. During acquisition, swimming distance and escape latency were comparable between groups [Figure 2B and C]. In the probe trial, target-quadrant distance, platform crossings, and target-quadrant duration did not differ significantly between groups [Figure 2D-F]. Accordingly, the MWM data do not provide evidence of improved spatial learning or memory.

Although the MWM outcomes were nonsignificant, the elevated plus maze showed a higher percentage of time spent in the open arms in *L. plantarum* L168-treated mice than in controls ($P = 0.0342$). The percentages of total distance traveled in the open arms ($P = 0.0722$) and total entries into the open arms ($P = 0.2277$) did not differ significantly between groups [Figure 2G-J]. This pattern was consistent with a possible reduction in anxiety-like behavior, as only one of the three EPM measures reached statistical significance. To assess whether gross locomotor differences might contribute to the behavioral results, we examined the available open-field data. The reported center- and peripheral-zone measures did not differ significantly between groups (Supplementary Figure 1B-G; all unadjusted $P > 0.29$). However, because absolute total-distance and velocity outcomes were not reported, locomotor confounding cannot be fully excluded.

Overall, long-term *L. plantarum* L168 supplementation did not improve spatial learning or memory in aged mice but showed a potential anxiolytic effect without apparent changes in the reported open-field measures. However, additional behavioral tests and comprehensive locomotor assessments are required to confirm this effect and exclude locomotor confounding.

Hippocampal RNA sequencing identifies treatment-associated expression differences

The behavioral findings prompted us to examine whether long-term *L. plantarum* L168 supplementation was accompanied by hippocampal transcriptional differences. RNA sequencing was performed on hippocampal tissue from five mice per group.

Principal component analysis showed partial separation between groups and substantial variability within the supplemented group [Figure 3A]. The heatmap displays expression profiles of 458 genes. Hierarchical clustering of these genes broadly distinguished the groups, with subsets showing higher or lower expression in supplemented mice [Figure 3B].

Gene Ontology analysis identified nominally enriched terms related to transcriptional regulation, RNA processing, innate and antiviral immune responses, extracellular matrix organization and BMP signaling [Figure 3C]. The representative-gene heatmap showed contrasting expression patterns, including higher expression of *Npas4*, *Shank1* and *Homer1* in supplemented mice [Figure 3D]. Figure 3E displays selected neural-system-related terms involving neuronal and glial differentiation, dendritic and synaptic organization, myelination, neuronal activity, memory and neuronal apoptosis.

Collectively, these findings indicate that long-term *L. plantarum* L168 supplementation is associated with broad hippocampal transcriptional differences involving neural and immune-related processes. However, these enrichment results are exploratory and do not establish pathway activation, neuroprotection, or a causal relationship with the observed behavioral phenotype.

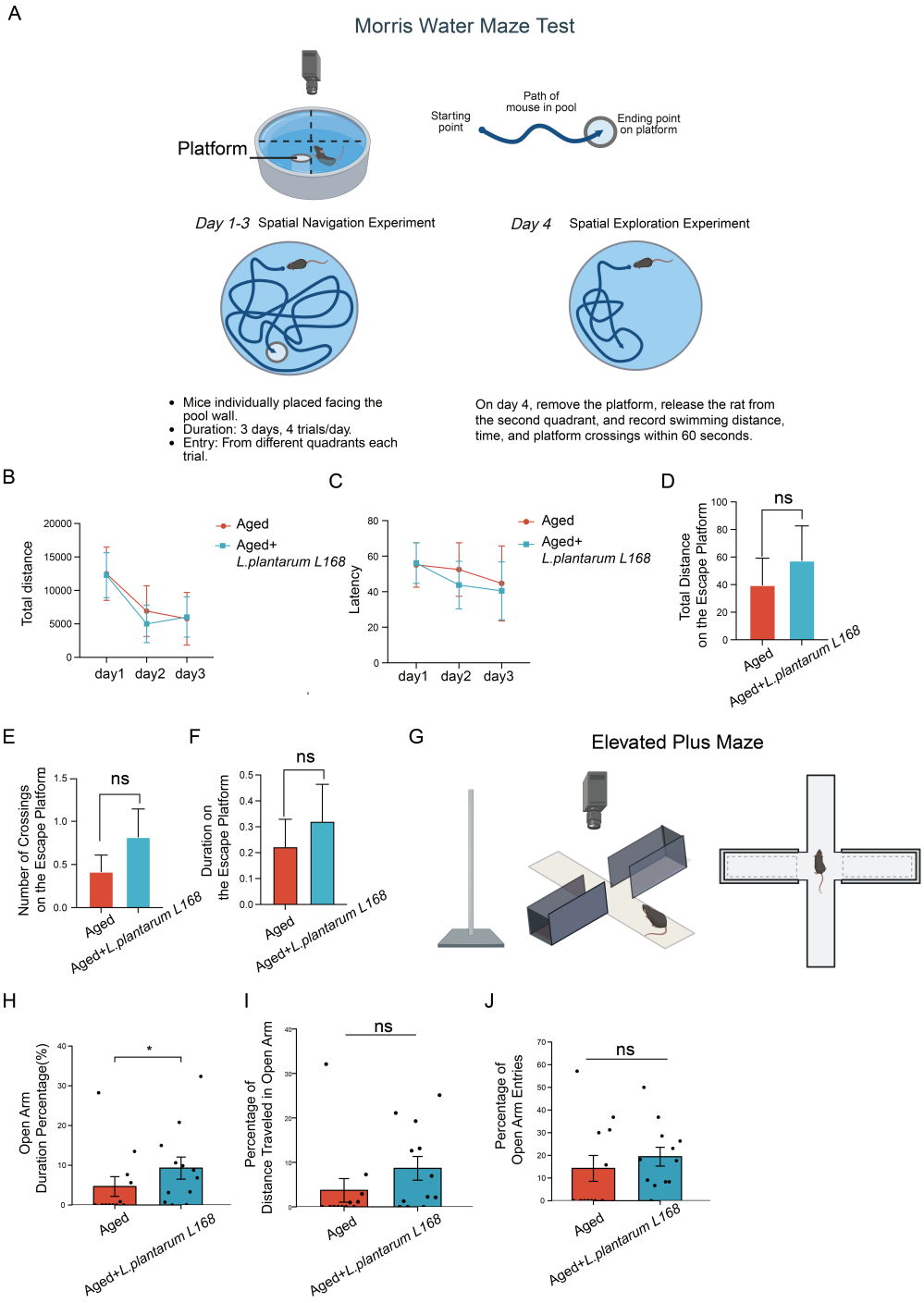

Figure 2. Behavioral outcomes after long-term *L. plantarum* L168 supplementation in aged mice. (A) Schematic representation of the MWM paradigm. For the spatial navigation phase (Days 1-3), mice were individually placed in the pool facing the wall and released from different quadrants across four trials per day, with a hidden escape platform located in the target quadrant. Each trial ended when the mouse reached the platform or after 60 s, in which case the mouse was guided to the platform. On Day 4, the platform was removed for the probe trial, in which mice were released from the opposite quadrant and allowed to swim freely for 60 s while swimming path, total distance in the target quadrant, time spent in the target quadrant, and number of crossings over the former platform location were recorded. Created with BioRender; (B and C) Total swimming distance (B; mm) and escape latency (C; s) during acquisition (aged control, $n = 12$; *L. plantarum* L168-supplemented, $n = 11$). Two-way repeated-measures ANOVA with treatment group and training day as factors showed, for swimming distance, a treatment-group effect of F (1, 21) = 0.553, $P = 0.4654$, a training-day effect of F (2, 42) = 25.122, $P = 6.68 \times 10^{-8}$, and a group × day interaction of F (2, 42) = 0.583, $P = 0.5624$. For escape latency, the corresponding values were F (1, 21) = 1.420, $P = 0.2467$, F (2, 42) = 3.747, $P = 0.0318$, and F (2, 42) = 0.531, $P = 0.5920$, respectively. P values are unadjusted; (D-F) Probe-trial performance, including total distance traveled in the target quadrant (D; mm; $P = 0.5759$), number of crossings over the former platform location (E; $P = 0.2909$), and duration in the target quadrant (F; s; $P = 0.5829$) (aged control, $n = 12$; *L. plantarum* L168-supplemented, $n = 11$). Unadjusted P values were calculated using unpaired two-tailed Student's t-tests. None of these between-group differences were statistically significant; (G) Schematic diagram of the EPM. Mice were placed at the center facing an open arm and allowed to explore for 5 min. Time spent in the open arms, distance traveled in the open arms, and number of open-arm entries were recorded. Created with BioRender; (H-J) EPM performance showing the percentage of total time spent in the open arms (H; $P = 0.0342$), percentage of total distance

traveled in the open arms (I; $P = 0.0722$), and percentage of total entries into the open arms (J; $P = 0.2277$) ($n = 12$ mice per group). Only the percentage of total time spent in the open arms reached statistical significance; the other two measures did not differ significantly between groups. *P* values are unadjusted and were calculated using unpaired two-tailed Student's *t*-tests. All data are presented as mean ± SEM. Panel-specific sample sizes are stated above. Symbols denote unadjusted *P* values: $^*P < 0.05$. ns: Not significant; EPM: elevated plus maze; SEM: standard error of the mean; MWM: Morris water maze; ANOVA: analysis of variance.

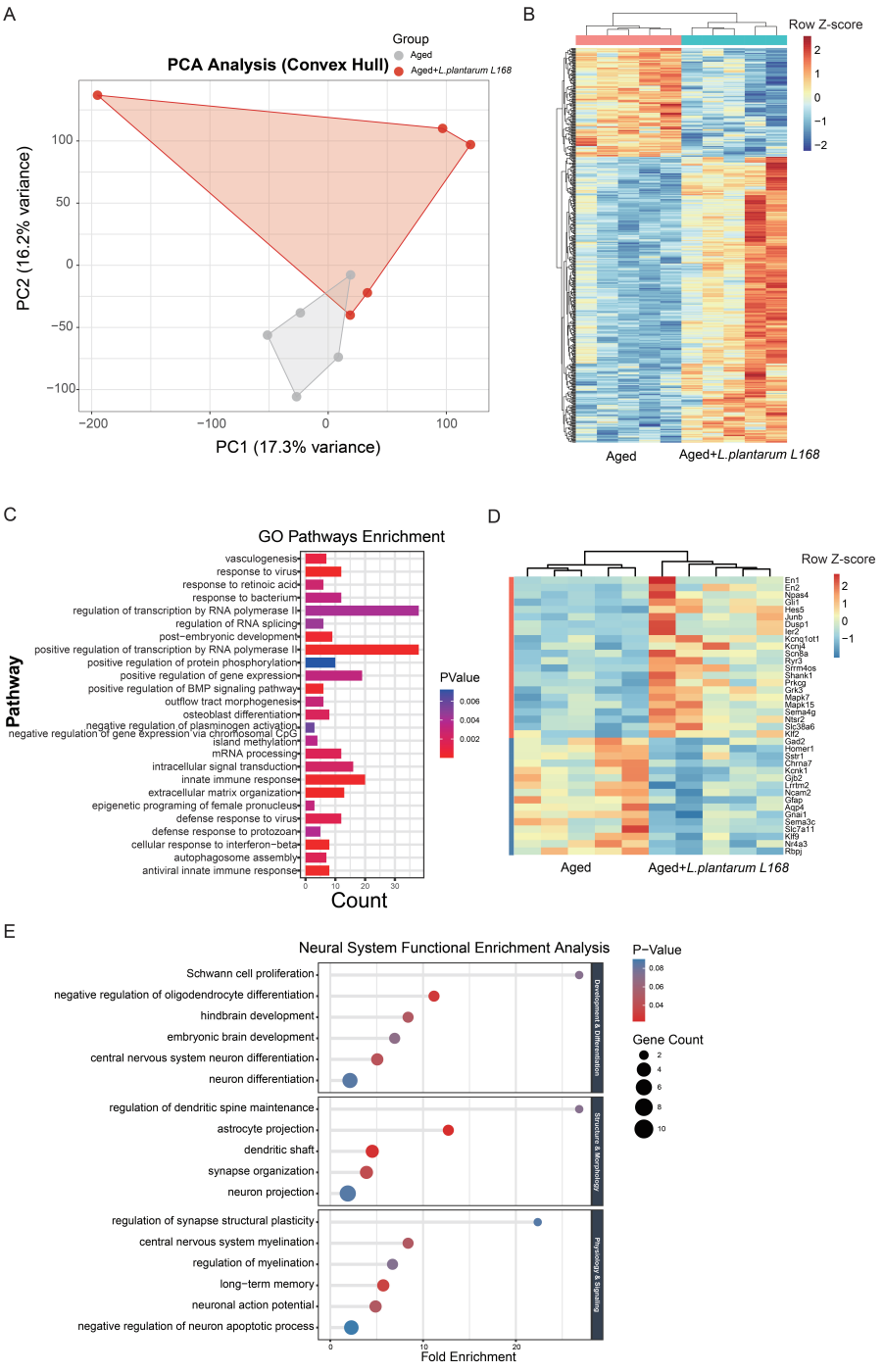

Figure 3. Hippocampal transcriptomic differences associated with long-term *L. plantarum* L168 supplementation in aged mice. (A) Principal component analysis of hippocampal gene-expression profiles ($n = 5$ mice/group; one independent library per mouse); (B) Heatmap showing the expression profiles of 458 genes across the 10 hippocampal samples. All displayed genes had $P < 0.05$ in the corresponding DESeq2 results; (C) Gene Ontology enrichment analysis of the differentially expressed genes using clusterProfiler v3.8.1; terms with unadjusted $P < 0.05$ were considered enriched; (D) Heatmap of representative differentially expressed genes from selected enriched pathways; (E) Focused display of selected neural-system-related GO terms. Dot size indicates gene count, color indicates the unadjusted *P* value, and the horizontal axis shows fold enrichment. Displayed terms are not all significant at $P < 0.05$. All panels include $n = 5$ mice per group, with one independent library per mouse; the mouse was the biological unit for all RNA-sequencing analyses. GO: Gene Ontology.

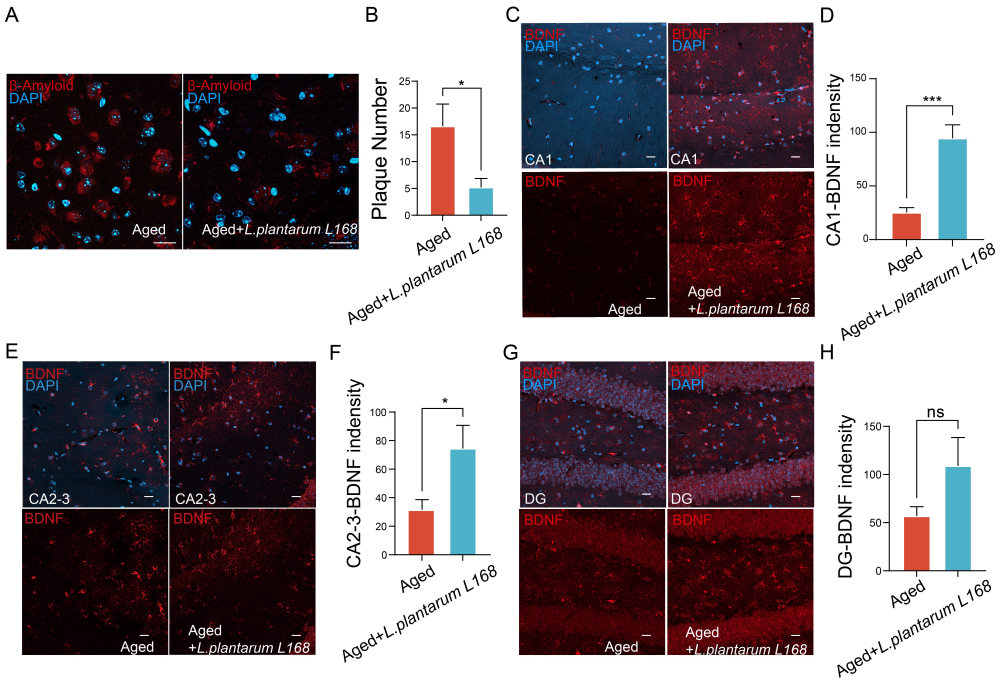

Figure 4. Hippocampal Aβ and BDNF immunofluorescence after *L. plantarum* L168 supplementation. (A) Representative hippocampal immunofluorescence images of Aβ immunoreactivity (red) and DAPI-stained nuclei (blue), acquired using a 40× objective. Scale bar, 20 μm; (B) Manual quantification of Aβ-immunoreactive deposits across the whole hippocampal region at the endpoint (n = 5 mice per group; one section and one mouse-level count per mouse; unpaired two-tailed Student's t-test, unadjusted P = 0.0335); (C, E and G) Representative immunofluorescence images of brain-derived neurotrophic factor (BDNF, red) in CA1 (C), CA2-3 (E), and DG (G), acquired using a 20× objective. Scale bars, 20 μm; (D, F and H) Mean BDNF fluorescence intensity in CA1 (D; P = 0.0008), CA2-3 (F; P = 0.0419) and DG (H; P = 0.1313), analyzed separately from complete Z-stacks acquired at 0.1-μm intervals (n = 5 mice per group; one section and one mouse-level value per subregion per mouse). Unadjusted P values were calculated using unpaired two-tailed Student's t-tests. All quantitative data in (B, D, F and H) are presented as mean ± SEM. BDNF fluorescence intensity was higher in CA1 and CA2-3 in the supplemented group, whereas the between-group difference in DG was not statistically significant. *P < 0.05; ***P < 0.001. ns: Not significant; BDNF: brain-derived neurotrophic factor; DAPI: 4′,6-diamidino-2-phenylindole; DG: dentate gyrus; Aβ: amyloid-β; SEM: standard error of the mean.

Long-term *L. plantarum* L168 supplementation is associated with reduced hippocampal Aβ accumulation and increased BDNF expression

The hippocampal transcriptomic analysis identified treatment-associated expression differences involving neural, synaptic, and immune-related processes. To determine whether these transcriptional differences were accompanied by tissue-level changes relevant to brain aging and neuronal function, we next compared hippocampal Aβ deposition and BDNF protein levels by immunofluorescence.

Aβ-immunoreactive deposits were detected in the hippocampi of aged control mice, whereas fewer deposits were observed in the *L. plantarum* L168-supplemented group at the study endpoint [Figure 4A and B]. Because Aβ levels were not measured before supplementation and its production and degradation were not directly assessed, this endpoint difference should not be interpreted as evidence of enhanced amyloid clearance.

We also assessed BDNF protein level by immunofluorescence, a marker relevant to synaptic plasticity and memory consolidation[37]. BDNF immunofluorescence differed by hippocampal region. The supplemented group showed higher BDNF fluorescence intensity in CA1 [Figure 4C and D] and CA2-3 [Figure 4E and F] than the aged control group. Although BDNF fluorescence intensity in the dentate gyrus (DG) showed a similar upward trend, the difference did not reach statistical significance [Figure 4G and H].

Together, these findings indicate that the hippocampal transcriptional differences associated with long-term *L. plantarum* L168 supplementation were accompanied by lower endpoint Aβ staining and region-specific increases in BDNF signals. However, these associations do not establish amyloid clearance, restoration of neurotrophic function, or a causal link to behavioral outcomes, particularly given the absence of detectable improvement in spatial learning and memory.

Long-term *L. plantarum* L168 supplementation is associated with improved colonic integrity and increased ZO-1 expression

Aging is associated with gut microbial dysbiosis, impaired barrier function, and low-grade systemic inflammation[10,38]. Because fecal samples were not collected during the animal experiment, longitudinal or luminal fecal microbiota profiling could not be performed. We therefore conducted an exploratory analysis of tissue-associated microbial DNA using paraffin-embedded colonic specimens, together with assessments of colonic morphology and epithelial integrity. Given the low microbial biomass of intestinal tissue and the potential effects of fixation, paraffin embedding, and background contamination on microbial DNA profiles, these microbiota findings should be interpreted cautiously.

The genus-level Shannon index did not differ between groups (two-sided Welch's *t*-test, $P = 0.511406$; Figure 5A). Genus-level Bray-Curtis-based PCoA showed overlapping group distributions, with no evidence of a between-group difference in overall community structure by PERMANOVA (999 permutations, $R^2 = 0.037$, $P = 0.7544$; Figure 5B). PERMDISP likewise found no evidence of a difference in multivariate dispersion between groups ($P = 0.863$). Group-mean phylum-level profiles were dominated by Pseudomonadota, Actinomycetota and Bacillota, with smaller contributions from Bacteroidota and Deferribacterota [Figure 5C]. The group-mean abundances of the 10 most abundant genera are shown in Figure 5D, with the remaining genera grouped as Others. Exploratory genus-level Wilcoxon tests identified nine taxa with nominal $P < 0.05$, which are displayed in the clustered heatmap [Figure 5E]. These findings suggest potential treatment-associated differences in specific genera despite the absence of a detectable difference in overall community structure. Because the genus-level comparisons were exploratory and were not adjusted for multiple testing, they should be interpreted as preliminary rather than confirmatory. PICRUSt2 analysis identified no predicted MetaCyc pathways that remained significant after false discovery rate (FDR) correction. Figure 5F shows the five pathways with the smallest nominal *P* values, but all Benjamini-Hochberg-adjusted *P* values were 1.00. *L. plantarum* L168 was not associated with broad community-wide restructuring but may have influenced the relative abundance of specific genera.

Despite the absence of detectable global microbial differences, *L. plantarum* L168 supplementation was associated with improved colonic tissue phenotypes. Colorectal length was modestly greater in *L. plantarum* L168-treated mice than in aged controls, although the difference was not statistically significant [Figure 5G and H].

H&E staining revealed epithelial injury and inflammatory-cell infiltration in aged controls, whereas *L. plantarum* L168-treated mice exhibited better-preserved mucosal morphology and significantly lower composite histopathology scores [Figure 5I and J].

Because ZO-1 is a tight-junction scaffolding protein[39], we next examined its expression and distribution. Aged controls exhibited weak and discontinuous epithelial ZO-1 staining, whereas *L. plantarum* L168-treated mice showed a more continuous epithelial distribution and significantly higher ZO-1 fluorescence intensity [Figure 5K and L].

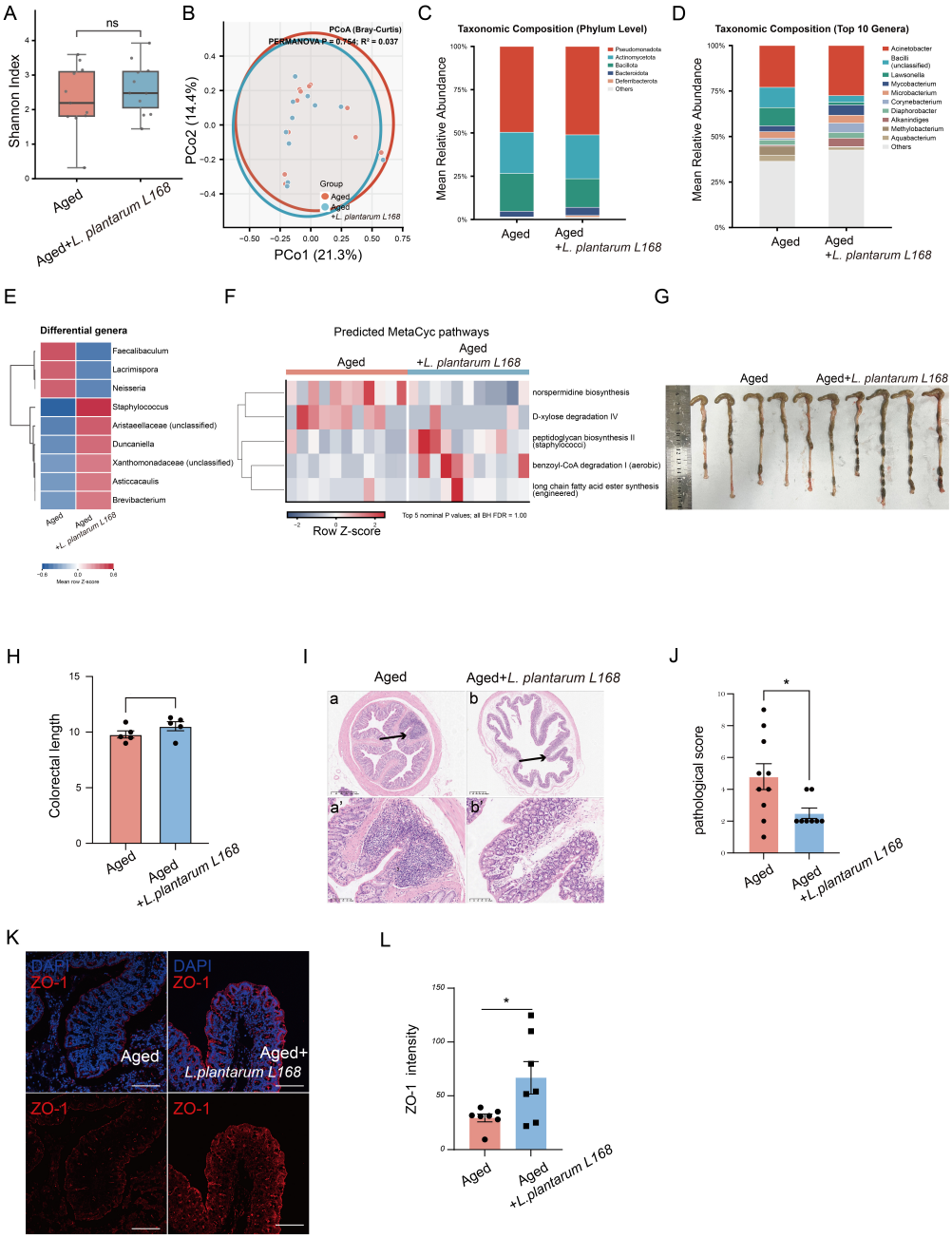

Figure 5. Tissue-associated microbiota, colonic histology, and ZO-1 immunofluorescence after *L. plantarum* L168 supplementation. (A) Alpha diversity of the tissue-associated microbiota profiled from formalin-fixed paraffin-embedded (FFPE) colon blocks, evaluated by the genus-level Shannon index (n = 11 mice per group; two-sided Welch's t-test, unadjusted P = 0.511406); (B) Principal coordinate analysis (PCoA) based on genus-level Bray-Curtis dissimilarity (PERMANOVA, 999 permutations, R^2 = 0.037, unadjusted P = 0.7544; PERMDISP, 999 permutations, unadjusted P = 0.863; n = 11 mice per group); (C) Group-mean relative abundance of the tissue-associated microbiota at the phylum level (n = 11 mice per group). Phyla with a mean relative abundance below 1% were grouped as 'Others'; (D) Group-mean relative abundance of the 10 most abundant genera across all samples; the remaining genera were grouped as 'Others' (n = 11 mice per group). Sample-level relative abundances of the displayed categories were compared between groups using two-sided Wilcoxon rank-sum tests; (E) Clustered heatmap of nine taxa meeting the nominal unadjusted $P < 0.05$ threshold in exploratory two-sided Wilcoxon rank-sum tests (n = 11 mice per group). No multiple-comparison correction was applied. Colors indicate mean row Z-scores, with red denoting relatively higher and blue denoting relatively lower abundance within each taxon; (F) Heatmap of the five PICRUSt2-inferred MetaCyc pathways with the smallest nominal P values in two-sided Wilcoxon rank-sum tests (n = 11 mice per group). P values were adjusted using the Benjamini-Hochberg procedure; all adjusted P values were 1.00. Colors indicate row Z-scores; (G) Representative macroscopic images of colons from the Aged and Aged+*L. plantarum* L168 groups; (H) Quantification of colorectal length (n = 5 mice per group; two-sided unpaired Student's t-test, unadjusted P = 0.1904); (I) Representative images of H&E-stained colon sections acquired using a NanoZoomer® S360 bright-field slide scanner with a 20× objective. Black arrows indicate areas of epithelial damage and inflammatory infiltration. Scale bars: 400 μm in the upper panels and 100 μm in the lower panels; (J) Composite histopathology scores based on H&E staining. Scores ranged from 0 to 16 and incorporated inflammation, tissue-structure damage, submucosal changes, glandular destruction and other special pathological changes. One section and one panoramic field were evaluated per mouse by a single observer blinded to group assignment (aged control, n = 10; *L. plantarum* L168-supplemented, n = 8; two-sided Mann-Whitney U test, unadjusted P = 0.0383);

(K) Representative immunofluorescence images of the tight-junction protein ZO-1 (red) and DAPI-stained nuclei (blue) in colon tissues. Images were acquired using a 40× objective; scale bar, 20 μm; (L) Quantification of ZO-1 fluorescence intensity (n = 7 mice per group; one section and one mouse-level full-Z-stack value per mouse; two-sided unpaired Student's t-test, unadjusted P = 0.0331). For panels (H, J and L) data are presented as mean ± SEM. *P < 0.05; Exact unadjusted P values are reported above. ns: Not significant; SEM: standard error of the mean; ZO-1: zonula occludens-1; H&E: hematoxylin and eosin; PERMDISP: permutational analysis of multivariate dispersions; PERMANOVA: permutational multivariate analysis of variance.

Collectively, *L. plantarum* L168 supplementation was associated with improved colonic histopathology and epithelial ZO-1 organization. Although global α-diversity and overall community structure did not differ significantly between groups, exploratory analyses identified nominal differences in nine genera, suggesting that *L. plantarum* L168 may be associated with changes in specific microbial taxa rather than broad community-wide restructuring. Because these genus-level comparisons were not adjusted for multiple testing and were based on microbial DNA obtained from paraffin-embedded colonic tissue, the findings remain preliminary and require validation using prospectively collected fecal or fresh intestinal samples.

L. plantarum L168 supplementation induced tissue-specific changes in cytokine-positive CD4⁺ T-cell frequencies

Aging is accompanied by alterations in T-cell composition and function, which may contribute to age-related immune dysregulation[40]. To determine whether *L. plantarum* L168 supplementation was associated with changes in CD4⁺ T-cell cytokine profiles, we quantified IL-4⁺, IL-17A⁺, and IFN-γ⁺ CD4⁺ T cells in the spleen and MLNs by flow cytometry. Representative splenic gating plots are provided in Supplementary Figures 2 and 3.

The frequency of IL-4⁺ CD4⁺ T cells in the spleen did not differ significantly between groups [Figure 6A and B]. In contrast, the frequency of IL-4⁺ CD4⁺ T cells in the MLNs was significantly higher in *L. plantarum* L168-supplemented mice than in aged controls [Figure 6C and D], indicating a tissue-specific difference in the IL-4-associated response. Representative flow-cytometry plots of IL-17A⁺ CD4⁺ T cells in the spleen and MLNs are shown in Figure 6E and F, respectively. No significant between-group differences in IL-17A⁺ CD4⁺ T-cell frequencies were detected in either tissue [Figure 6G and H].

Representative plots of IFN-γ⁺ CD4⁺ T cells in the spleen and MLNs are shown in Figure 6I and J. *L. plantarum* L168-supplemented mice exhibited a significantly lower frequency of splenic IFN-γ⁺ CD4⁺ T cells than aged controls, whereas the corresponding frequency in the MLNs did not differ significantly between groups [Figure 6K and L].

Collectively, these findings indicate that *L. plantarum* L168 supplementation was associated with selective and tissue-dependent changes in cytokine-positive CD4⁺ T-cell populations, characterized by a higher frequency of IL-4⁺ CD4⁺ T cells in the MLNs and a lower frequency of IFN-γ⁺ CD4⁺ T cells in the spleen, without detectable changes in IL-17A⁺ CD4⁺ T-cell frequencies. Because cytokine positivity alone does not define stable T-cell lineages or their overall inflammatory functions, these results should not be interpreted as evidence of a uniform shift toward either a pro-inflammatory or an anti-inflammatory immune state.

DISCUSSION

This study evaluated the effects of 12 months of *L. plantarum* L168 supplementation in naturally aged female mice using untreated age-matched mice as controls. Across behavioral, transcriptomic, histological, immunofluorescence, microbiome, and flow cytometric assessments, *L. plantarum* L168-supplemented mice showed favorable changes in several outcomes, including lower body weight at the study endpoint, improved colonic histopathology and epithelial ZO-1 expression, longer open-arm time in the elevated plus maze, shifts in selected tissue-associated microbial genera, tissue-dependent changes in cytokine-positive CD4⁺

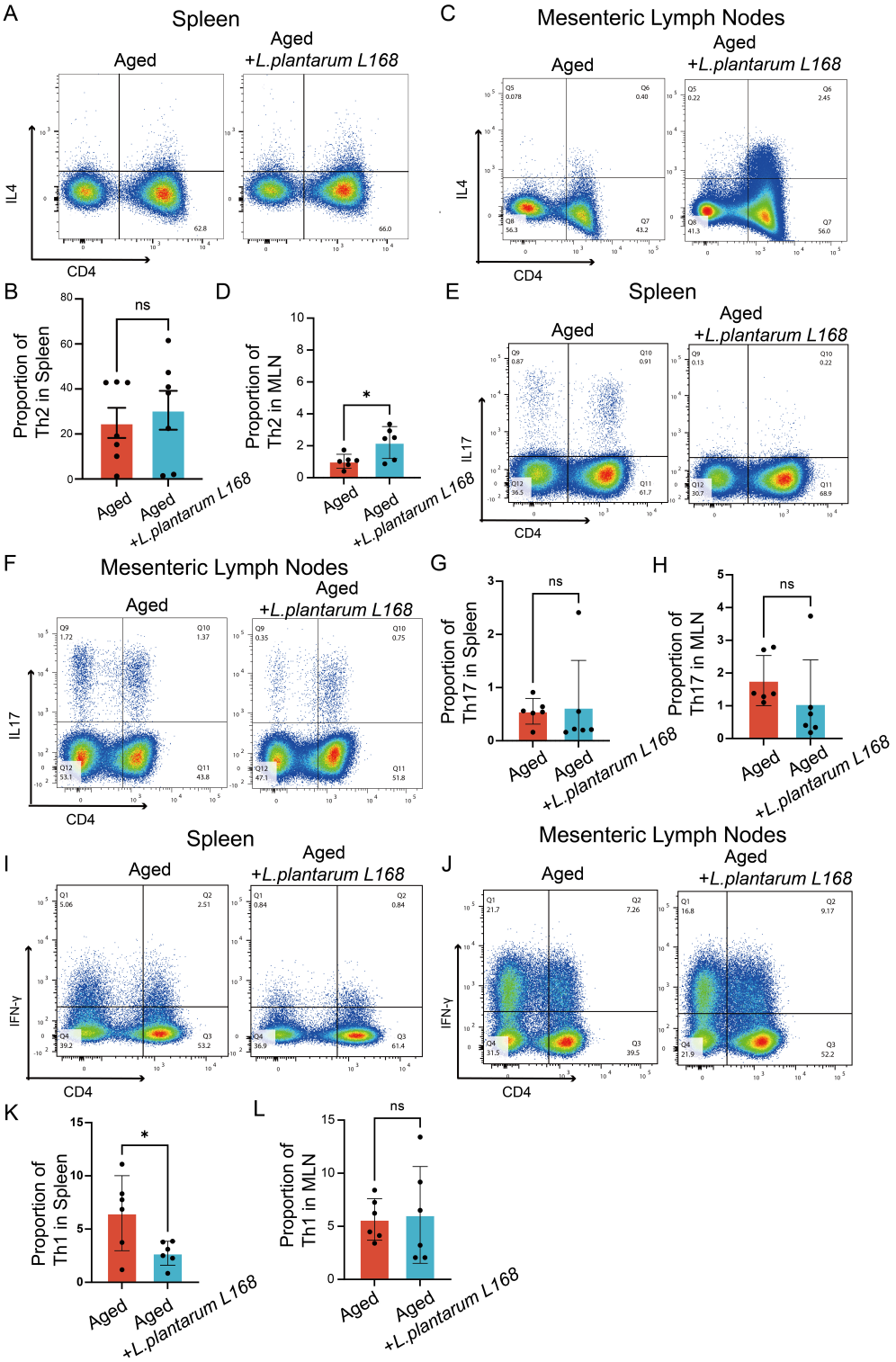

Figure 6. Cytokine-positive CD4⁺ T-cell frequencies in the spleen and mesenteric lymph nodes of aged mice. (A and B) Representative flow cytometry plots (A) and quantification (B) of IL-4-positive CD4⁺ T cells in the spleen. The between-group difference was not statistically significant (n = 6 mice per group; two-sided unpaired Student's t-test, P = 0.5831); (C and D) Representative plots (C) and quantification (D) of IL-4-positive CD4⁺ T cells in the MLN (n = 6 mice per group; two-sided unpaired Student's t-test, P = 0.0248). The frequency was higher in the supplemented group; (E and F) Representative plots of IL-17A-positive CD4⁺ T cells in the spleen (E) and MLN (F); n = 6 mice per group; (G and H) Quantification of IL-17A-positive CD4⁺ T-cell frequencies in the spleen (G; P = 0.8556) and MLN (H; P = 0.2857) (n = 6 mice per group; two-sided unpaired Student's t-tests). Neither comparison was statistically significant; (I and J) Representative plots of IFN-γ-positive CD4⁺ T cells in the spleen (I) and MLN (J); n = 6 mice per group; (K and L) Quantification of IFN-γ-positive CD4⁺ T-cell frequencies in the spleen (K; P = 0.0318) and MLN (L; P = 0.8399) (n = 6 mice per group; two-sided unpaired Student's t-tests). The splenic frequency was lower in the supplemented group; the MLN comparison was not significant. For all quantified panels, frequencies represent the percentage of live CD45⁺CD3⁺ cells co-expressing CD4 and the indicated cytokine. Data are presented as mean ± SEM. P values are unadjusted. *P < 0.05. ns: Not significant; IL: interleukin; MLN: mesenteric lymph node; CD4: cluster of

differentiation 4; IFN-γ: interferon-gamma; SEM: standard error of the mean.

T-cell frequencies, and differences in hippocampal staining and gene expression. Together, these findings indicate that long-term *L. plantarum* L168 supplementation might improve specific aging-related phenotypes in naturally aged female mice. Future studies incorporating young reference groups and longitudinal assessments may further clarify whether these effects extend to the rate or trajectory of aging.

Aging is frequently accompanied by chronic low-grade inflammation, and age-related intestinal barrier dysfunction may contribute to systemic inflammatory signaling[10,38]. *L. plantarum* L168 supplementation was associated with higher colonic ZO-1 fluorescence and lower histopathological scores. Colorectal length did not differ significantly between the two aged groups, and higher ZO-1 fluorescence alone does not establish restoration of functional intestinal permeability. The concurrent differences in cytokine-positive $CD4^+$ T-cell frequencies may be related, but the present design does not establish a causal link between the intestinal and immune findings.

The "gut-brain axis" hypothesis posits that gut microbes influence the central nervous system via immune, neural, and metabolic pathways[41,42]. Our results showed greater open-arm time in the elevated plus maze and higher BDNF expression in selected hippocampal regions after *L. plantarum* L168 supplementation, but they do not establish neuroprotection or cognitive improvement. One possible mechanism involves microbial metabolites acting as epigenetic modulators[13,15,43].

Previous studies have linked aging-related cognitive decline to changes in neuroinflammatory and metabolic pathways[44]. In our study, supplementation was associated with higher expression of selected genes, including Npas4, Shank1 and Homer1 [Figure 3D]. This expression pattern is consistent with altered synaptic gene regulation but does not demonstrate structural remodeling or stronger neural connectivity. These observations raise the hypothesis that *L. plantarum* L168-related metabolites influence hippocampal gene regulation. This hypothesis requires direct testing.

The study has several limitations. First, female mice were selected to reduce aggression-related injury and attrition during prolonged group housing. However, the single-sex design did not allow assessment of sex-dependent responses and limits the generalizability of the findings to males; studies in male cohorts are therefore needed. Although untreated age-matched controls enabled direct assessment of *L. plantarum* L168-associated effects, the study did not include a young reference group or pretreatment measurements for most outcomes. Accordingly, the conclusions concern improvements relative to untreated aged female controls, while young reference groups and longitudinal measurements would provide additional context for interpreting these changes across the aging process. Second, the absence of longitudinal body weight data, food and water intake records, body composition measurements, and quantitative assessment of fur condition limits the interpretation of the gross phenotypic findings. Future studies should include these measures to provide a more complete assessment of treatment-associated physical changes during aging. Water consumption and viable *L. plantarum* L168 concentrations throughout the 48-h replacement interval should also be monitored to better define actual exposure. Third, although five-region 16S rRNA sequencing of FFPE colon sections was used to characterize the mucosa-associated microbiota *in situ*, this approach has inherent limitations. Formalin fixation can cause DNA cross-linking and fragmentation, potentially introducing amplification bias and reducing the detection of low-abundance taxa despite the multiplexed amplification strategy. Moreover, this localized endpoint profile of the tissue-associated microbiota may not fully reflect broader changes in the luminal or fecal microbiome. Fourth, the genus-level findings were based on unadjusted exploratory analyses, and none of the PICRUSt2 pathways remained significant after Benjamini–Hochberg correction. The observed amyloid immunoreactivity was not confirmed using an

independent analytical method, and intestinal permeability was not assessed using a functional assay. In addition, the absence of direct metabolomic and functional validation means that the predicted pathways should be regarded as hypothesis-generating findings rather than evidence of altered metabolic activity or causal metabolites. Future studies combining metagenomics, metabolomics, functional intestinal barrier assays, age-referenced controls, and longitudinal measurements are needed to investigate the underlying mechanisms and the relevance of these findings to healthy aging.

In summary, long-term *L. plantarum* L168 supplementation was associated with favorable changes in several outcomes relevant to aging in naturally aged female mice. These changes included improved colonic histopathology and epithelial ZO-1 organization, shifts in selected tissue-associated microbial genera, tissue-dependent differences in cytokine-positive $CD4^+$ T-cell frequencies, and changes in selected behavioral and hippocampal measures. However, performance in the MWM was not significantly improved, and the exploratory microbiota findings should be interpreted cautiously because they were derived from paraffin-embedded colonic tissue rather than prospectively collected fecal or fresh intestinal samples. Moreover, the endpoint analyses did not establish functional restoration of intestinal permeability or demonstrate reversal of immunosenescence, cognitive decline, or aging itself. Future studies incorporating young reference groups, longitudinal sampling, direct functional measurements, and mechanistic investigations are needed to determine the biological significance of these changes and whether *L. plantarum* L168 can support specific aspects of healthy aging.

DECLARATIONS

Acknowledgements

The Graphical Abstract was created with BioRender.

Authors' contributions

Conceived, designed and supervised the project: Liu X
Led the experimental work and conducted the RNA-seq and five-region 16S rRNA gene analyses: Pei Y
Performed the flow cytometry experiments: Wang J, Pei Y
Contributed to the experimental work: Ni S, Yang J, Chen R, Liu Y, Pei Y
Organized the figures: Luan X, Wang J, Pei Y
Drafted the **METHODS** section: Pei Y, Luan X
Provided critical input during manuscript preparation: Wang J, Pei Y
Drafted the manuscript and led the revision process: Luan X, Pei Y
Revised the manuscript: Luan X, Pei Y, Wang J
Participated in manuscript revision: Shen X
Reviewed the language, spelling and formatting and provided substantive comments on the experimental methods, interpretation of the **RESULTS** and **DISCUSSION**: Luan X, Huang W
All authors validated the work and approved the final manuscript.

Availability of data and materials

The five-region 16S rRNA gene-sequencing dataset, including sequencing data for all 15 negative controls, has been deposited in the China National GeneBank DataBase (CNGBdb; https://db.cngb.org/) under project accession number CNP0010225. The hippocampal RNA-sequencing dataset has been deposited in the same repository under project accession number CNP0010032.

AI and AI-assisted tools statement

During the preparation of this manuscript, the AI tool ChatGPT (model version GPT-6.1-sol, released 2026-09-29) was used solely for language editing. The tool did not influence the study design, data collection, analysis, interpretation, or the scientific content of the work. All authors take full responsibility for the accuracy, integrity, and final content of the manuscript.

Financial support and sponsorship

This work was supported by the National Natural Science Foundation of China (NSFC grant 82301773).

Conflicts of interest

Nanjing Medical University assigned Chinese patent CN114404457B, which covers the use of *Lactiplantibacillus plantarum* L168 in the preparation of a drug to delay ovarian aging, to Beijing Qunfeng Nayuan Health Technology Co., Ltd. The patent describes experiments conducted in a fruit fly model. Nanjing Medical University, Liu X, Pei Y, Wang J, Luan X, Liu Y and Chen R received proceeds from the patent assignment. The company did not provide financial support for the present study. The authors declare no other conflicts of interest.

Ethical approval and consent to participate

All animal experiments were conducted in accordance with protocols approved by the Institutional Animal Care and Use Committee of Nanjing Medical University (Approval No. IACUC-2006031).

Copyright

© The Author(s) 2026.

Supplementary Materials

Supplementary Materials

REFERENCES

1. Brito DVC, Esteves F, Rajado AT, et al.; ALFA score Consortium. Assessing cognitive decline in the aging brain: lessons from rodent and human studies. *npj Aging.* 2023;9:120. DOI PubMed PMC
2. Ginefra P, Hope HC, Lorusso G, D'amelio P, Vannini N. The immunometabolic roots of aging. *Curr Opin Immunol.* 2024;91:102498. DOI PubMed
3. Saleh Z, Mirzazadeh S, Mirzaei F, Heidarnejad K, Meri S, Kalantar K. Alterations in metabolic pathways: a bridge between aging and weaker innate immune response. *Front Aging.* 2024;5:1358330. DOI PubMed PMC
4. Guo J, Huang X, Dou L, et al. Aging and aging-related diseases: from molecular mechanisms to interventions and treatments. *Sig Transduct Target Ther.* 2022;7:1251. DOI PubMed PMC
5. Tenchov R, Sasso JM, Wang X, Zhou QA. Aging hallmarks and progression and age-related diseases: a landscape view of research advancement. *ACS Chem Neurosci* 2024;15:1-30. DOI PubMed PMC
6. Jing Y, Wang Q, Bai F, et al. Age-related alterations in gut homeostasis are microbiota dependent. *npj Biofilms Microbiomes.* 2025;11:677. DOI PubMed PMC
7. N V K, M S. Aging through the lens of the gut microbiome: challenges and therapeutic opportunities. *Arch Gerontol Geriatr Plus.* 2025;2:100142. DOI
8. Wu H, Wu E. The role of gut microbiota in immune homeostasis and autoimmunity. *Gut Microbes.* 2012;3:4-14. DOI PubMed PMC
9. Clark RI, Walker DW. Role of gut microbiota in aging-related health decline: insights from invertebrate models. *Cell Mol Life Sci* 2018;75:93-101. DOI PubMed PMC
10. Thevaranjan N, Puchta A, Schulz C, et al. Age-associated microbial dysbiosis promotes intestinal permeability, systemic inflammation, and macrophage dysfunction. *Cell Host Microbe.* 2017;21:455-466.e4. DOI PubMed PMC
11. Xiao Y, Feng Y, Zhao J, Chen W, Lu W. Achieving healthy aging through gut microbiota-directed dietary intervention: focusing on microbial biomarkers and host mechanisms. *J Adv Res.* 2025;68:179-200. DOI PubMed PMC
12. Zeng Z, Huang Z, Yue W, Nawaz S, Chen X, Liu J. Lactobacillus plantarum modulate gut microbiota and intestinal immunity in cyclophosphamide-treated mice model. *Biomed Pharmacother.* 2023;169:115812. DOI
13. Zhang Q, Zhao Q, Li T, et al. Lactobacillus plantarum-derived indole-3-lactic acid ameliorates colorectal tumorigenesis via epigenetic regulation of CD8+ T cell immunity. *Cell Metab.* 2023;35:943-960.e9. DOI
14. Shen X, Yang Z, Wang Q, et al. Lactobacillus plantarum L168 improves hyperoxia-induced pulmonary inflammation and hypoalveolarization in a rat model of bronchopulmonary dysplasia. *npj Biofilms Microbiomes.* 2024;10:504. DOI PubMed PMC
15. Li T, Chen J, Mi K, et al. Probiotics derived sodium benzoate improves social behavior of offspring exposed in the maternal immune activation through regulation of histone lysine benzoylation in astrocytes. *Mol Psychiatry.* 2025;30:5849-64. DOI PubMed PMC
16. Huang W, Wang X, Su Z, Chen X, Mao X, Liu X. Probiotic characteristics and whole genome sequence analysis of Lactiplantibacillus plantarum L168. *Food Biosci* 2025;70:107044. DOI
17. Morris R. Developments of a water-maze procedure for studying spatial learning in the rat. *J Neurosci Methods.* 1984;11:47-60. DOI

18. Vorhees CV, Williams MT. Morris water maze: procedures for assessing spatial and related forms of learning and memory. *Nat Protoc.* 2006;1:848-58. DOI PubMed PMC
19. Pellow S, Chopin P, File SE, Briley M. Validation of open: closed arm entries in an elevated plus-maze as a measure of anxiety in the rat. *J Neurosci Methods.* 1985;14:149-67. DOI
20. Walf AA, Frye CA. The use of the elevated plus maze as an assay of anxiety-related behavior in rodents. *Nat Protoc.* 2007;2:322-8. DOI PubMed PMC
21. Kraeuter A, Guest PC, Sarnyai Z. The open field test for measuring locomotor activity and anxiety-like behavior. In: Guest PC, editor. Pre-clinical models. New York: Springer; 2019. pp. 99-103. DOI
22. Seibenhener ML, Wooten MC. Use of the open field maze to measure locomotor and anxiety-like behavior in mice. *JoVE* 2015. DOI PubMed PMC
23. Fuks G, Elgart M, Amir A, et al. Combining 16S rRNA gene variable regions enables high-resolution microbial community profiling. *Microbiome.* 2018;6:396. DOI PubMed PMC
24. Mcdonald D, Jiang Y, Balaban M, et al. Greengenes2 unifies microbial data in a single reference tree. *Nat Biotechnol.* 2024;42:715-8. DOI PubMed PMC
25. Douglas GM, Maffei VJ, Zaneveld JR, et al. PICRUSt2 for prediction of metagenome functions. *Nat Biotechnol.* 2020;38:685-8. DOI PubMed PMC
26. Chen S, Zhou Y, Chen Y, Gu J. Fastp: an ultra-fast all-in-one FASTQ preprocessor. *Bioinformatics.* 2018;34:i884-90. DOI PubMed PMC
27. Kim D, Paggi JM, Park C, Bennett C, Salzberg SL. Graph-based genome alignment and genotyping with HISAT2 and HISAT-genotype. *Nat Biotechnol.* 2019;37:907-15. DOI PubMed PMC
28. Liao Y, Smyth GK, Shi W. featureCounts: an efficient general purpose program for assigning sequence reads to genomic features. *Bioinformatics.* 2014;30:923-30. DOI PubMed
29. Love MI, Huber W, Anders S. Moderated estimation of fold change and dispersion for RNA-seq data with DESeq2. *Genome Biol.* 2014;15:550. DOI PubMed PMC
30. Yu G, Wang L, Han Y, He Q. clusterProfiler: an R package for comparing biological themes among gene clusters. *OMICS.* 2012;16:284-7. DOI PubMed PMC
31. Mattson MP, Arumugam TV. Hallmarks of brain aging: adaptive and pathological modification by metabolic states. *Cell Metab.* 2018;27:1176-99. DOI PubMed PMC
32. Hou Y, Dan X, Babbar M, et al. Ageing as a risk factor for neurodegenerative disease. *Nat Rev Neurol.* 2019;15:565-81. DOI
33. Bettio LE, Rajendran L, Gil-Mohapel J. The effects of aging in the hippocampus and cognitive decline. *Neurosci Biobehav Rev.* 2017;79:66-86. DOI PubMed
34. Lee DY, Shin YJ, Kim JK, Jang HM, Joo MK, Kim DH. Alleviation of cognitive impairment by gut microbiota lipopolysaccharide production-suppressing *Lactobacillus plantarum* and *Bifidobacterium longum* in mice. *Food Funct.* 2021;12:10750-63. DOI PubMed
35. Lotfy WA, Ali AM, Abdou HM, Ghanem KM. Neuroprotective and probiotic potential of *Lactiplantibacillus plantarum* AM2 in cognitive impairment. *Sci Rep.* 2025;15:6103. DOI PubMed PMC
36. Di Salvo C, D'Antongiovanni V, Benvenuti L, et al. *Lactiplantibacillus plantarum* HEAL9 attenuates cognitive impairment and progression of Alzheimer's disease and related bowel symptoms in SAMP8 mice by modulating microbiota-gut-inflammasome-brain axis. *Food Funct* 2024;15:10323-38. DOI PubMed
37. Lu B, Nagappan G, Guan X, Nathan PJ, Wren P. BDNF-based synaptic repair as a disease-modifying strategy for neurodegenerative diseases. *Nat Rev Neurosci.* 2013;14:401-16. DOI PubMed
38. Man AL, Bertelli E, Rentini S, et al. Age-associated modifications of intestinal permeability and innate immunity in human small intestine. *Clin Sci (Lond).* 2015;129:515-27. DOI
39. Zihni C, Mills C, Matter K, Balda MS. Tight junctions: from simple barriers to multifunctional molecular gates. *Nat Rev Mol Cell Biol.* 2016;17:564-80. DOI PubMed
40. Goronzy JJ, Weyand CM. Mechanisms underlying T cell ageing. *Nat Rev Immunol.* 2019;19:573-83. DOI PubMed PMC
41. Cryan JF, Dinan TG. Mind-altering microorganisms: the impact of the gut microbiota on brain and behaviour. *Nat Rev Neurosci.* 2012;13:701-12. DOI PubMed
42. Cryan JF, O'Riordan KJ, Cowan CSM, et al. The microbiota-gut-brain axis. *Physiol Rev* 2019;99:1877-2013. DOI PubMed
43. Krautkramer KA, Fan J, Bäckhed F. Gut microbial metabolites as multi-kingdom intermediates. *Nat Rev Microbiol.* 2021;19:77-94. DOI PubMed
44. Minhas PS, Latif-Hernandez A, Mcreynolds MR, et al. Restoring metabolism of myeloid cells reverses cognitive decline in ageing. *Nature.* 2021;590:122-8. DOI PubMed PMC

Disclaimer/Publisher's Note: All statements, opinions, and data contained in this publication are solely those of the individual author(s) and contributor(s) and do not necessarily reflect those of OAE and/or the editor(s). OAE and/or the editor(s) disclaim any responsibility for harm to persons or property resulting from the use of any ideas, methods, instructions, or products mentioned in the content.

© The Author(s) 2026. Open Access This article is licensed under a Creative Commons Attribution 4.0 International License (https://creativecommons.org/licenses/by/4.0/), which permits unrestricted use, sharing, adaptation, distribution and reproduction in any medium or format, for any purpose, even commercially, as long as you give appropriate credit to the original author(s) and the source, provide a link to the Creative Commons license, and indicate if changes were made.